

Regulating the selective adsorption of OH* over equatorial position of Co₃O₄ via doping of Ru ions for efficient water oxidation reaction

Ragunath Madhu,^{a,b} Arun Karmakar,^{a,b} Preethi Arunachalam,^{c,#} Jaisakthi

Muthukumar,^{c,#} Pradeep Gudlur^d and Subrata Kundu^{a,b,*}

^aAcademy of Scientific and Innovative Research (AcSIR), Ghaziabad-201002, India.

^bElectrochemical Process Engineering (EPE) Division, CSIR-Central Electrochemical Research Institute (CECRI), Karaikudi-630003, Tamil Nadu, India.

^cCentre for Education (CFE), CSIR-Central Electrochemical Research Institute (CECRI), Karaikudi 630 003, Tamil Nadu, India.

^dDepartment of Mechanical Engineering, Union College, 807 Union Street Schenectady, NY, 12308, USA.

*To whom correspondence should be addressed, *E-mail:* skundu@cecri.res.in; kundu.subrata@gmail.com. Phone/Fax: (+ 91) 4565-241487.

This file contains 34 pages in which the information on reagents and instruments used in the study, electrochemical measurements, surface charge determination, XRD, XPS, BET and other electrochemical calculations like ECSA, C_{dl} values, etc., comparison table, references are given respectively.

Number of Figures: 14 (S1-S14)

Number of Tables: 4 (S1-S4)

Figures & tables	Subject of the Figure	Page number
S1	PXRD pattern of Co-BTC	S9
S2	Deconvoluted O 1s XPS spectra of Co ₃ O ₄ , Ru-Co ₃ O ₄ 10, Ru-Co ₃ O ₄ 15 and Ru-Co ₃ O ₄ 20.	S10
S3	N ₂ adsorption-desorption of Co ₃ O ₄ , Ru-Co ₃ O ₄ 10, Ru-Co ₃ O ₄ 15 and Ru-Co ₃ O ₄ 20 respectively.	S11
S4	LSV polarization result of commercial RuO ₂ in 1 M KOH electrolyte.	S12
S5	CVs recorded at non-faradaic region at a different scan rate for Co ₃ O ₄ , Ru-Co ₃ O ₄ 10, Ru-Co ₃ O ₄ 15 and Ru-Co ₃ O ₄ 20 respectively in 1 M KOH electrolyte.	S13
S6	ECSA normalized and mass dependent activity of Co ₃ O ₄ , Ru-Co ₃ O ₄ 10, Ru-Co ₃ O ₄ 15 and Ru-Co ₃ O ₄ 20 respectively in 1 M KOH.	S14
S7	Operando Nyquist plot of Co ₃ O ₄ , Ru-Co ₃ O ₄ 10, Ru-Co ₃ O ₄ 15 and Ru-Co ₃ O ₄ 20 respectively	S15
S8	Faradaic efficiency (FE) of the Ru-Co ₃ O ₄ 15 electrocatalyst for OER in 1 M KOH solution.	S16
S9	LSV polarization curves of Ru-Co ₃ O ₄ 15 after 1000 continuous CV cycles in 1 M KOH solution and corresponding EIS analysis.	S17
S10	Redox feature of Co ₃ O ₄ , Ru-Co ₃ O ₄ 10, Ru-Co ₃ O ₄ 15 and Ru-Co ₃ O ₄ 20 respectively measured at 100 mV/s.	S18
S11	LSV polarization result of commercial RuO ₂ in 0.5 M H ₂ SO ₄ electrolyte.	S19
S12	CVs recorded at non-faradaic region at a different scan rate for Co ₃ O ₄ , Ru-Co ₃ O ₄ 10, Ru-Co ₃ O ₄ 15 and Ru-Co ₃ O ₄ 20 respectively in 0.5 M H ₂ SO ₄ electrolyte.	S20
S13	ECSA normalized and mass dependent activity of Co ₃ O ₄ , Ru-Co ₃ O ₄ 10, Ru-Co ₃ O ₄ 15 and Ru-Co ₃ O ₄ 20 respectively in 0.5 M H ₂ SO ₄	S21
S14	LSV polarization curves of Ru-Co ₃ O ₄ 15 after 1000 continuous CV cycles in 0.5 M H ₂ SO ₄ solution and corresponding EIS analysis.	S22
S15	Post XRD analysis of Ru-Co ₃ O ₄ 15	S23
S16	Post Raman analysis of Ru-Co ₃ O ₄ 15 in 0.5 M H ₂ SO ₄ solution	S24
S17	Post XPS analysis of Ru-Co ₃ O ₄ 15	S25
S18	Post HR-TEM analysis of Ru-Co ₃ O ₄ 15 in 1 M KOH solution	S26
S19	Post HR-TEM analysis of Ru-Co ₃ O ₄ 15 in 0.5 M H ₂ SO ₄ electrolyte	S27
S20	Optimized electronic structure of Co ₃ O ₄ and Ru-Co ₃ O ₄	S28
S21	Determination of bond length before and after doping of Ru towards Co ₃ O ₄ respectively.	S29
Table S1	TOF values calculated at 350 and 370 mV overpotential for Co ₃ O ₄ and	S30

	various Ru-Co ₃ O ₄ catalyst.	
Table S2	Comparative electrochemical outcomes of Co ₃ O ₄ and various Ru-Co ₃ O ₄ catalyst.	S30
Table S3	Comparison of electrocatalytic performance of as-prepared Ru-Co ₃ O ₄ 15 with the similar reported electrocatalyst in 1 M KOH medium.	S31
Table S4	Comparison of electrocatalytic performance of as-prepared Ru-Co ₃ O ₄ 15 with the similar reported electrocatalyst in 0.5 M H ₂ SO ₄ medium.	S32
	References	S33

Experimental Section

Reagents used

Cobalt acetate tetrahydrate ($\text{Co}(\text{OAc})_2 \cdot 4\text{H}_2\text{O}$), Ruthenium chloride hydrate ($\text{RuCl}_3 \cdot x\text{H}_2\text{O}$), Polyvinylpyrrolidone ($(\text{C}_6\text{H}_9\text{NO})_6$, PVP), Benzene-1,3,5-Benzenetricarboxylic acid ($\text{C}_9\text{H}_6\text{O}_6$, BTC), ethanol ($\text{C}_2\text{H}_5\text{OH}$) were purchased from the Sigma-Aldrich and used as received. Deionized water (DI) is used throughout this work.

Synthesis of Co-BTC derived Co_3O_4

The Co-BTC particles were synthesized by following the previous reported research article by using MOF as precursor. Typically, 0.15 g of cobalt acetate tetrahydrate and 0.6 g of polyvinylpyrrolidone were dissolved in (1:1) ratio of deionized water and ethanol mixture and marked as solution (I). 180 mg of Benzene-1,3,5-Benzenetricarboxylic acid (BTC) was dissolved in (1:1) ratio of deionized water and ethanol mixture and marked as solution (II). Then the solution (II) was added dropwise and stirred for 15 min and aged for 24 h at room temperature. Then the obtained precipitate was collected, centrifuged, and washed with DI water and ethanol mixture for three times and dried in a hot air oven at 60 °C for 12 h. Then the obtained Co-BTC was annealed at 350 °C for 4 h at a ramping rate of 5°C/min in an air atmosphere. The obtained black powder was represented and named as Co_3O_4 .

Synthesis of Ru doped Co_3O_4

Briefly, 90 mg of prepared Co_3O_4 particles was dispersed in a (1:1) ratio of deionized water and ethanol mixture where 0.010 g/L of $\text{RuCl}_3 \cdot x\text{H}_2\text{O}$ solution was added and stirred for homogeneity. Then the obtained solution was transferred to a stainless-steel Teflon autoclave and maintained at 120 °C for 12 h. The obtained precipitate was centrifuged and washed several times with water and dried in a hot air oven at 60 °C for 12 h, named as Ru- Co_3O_4 10. Likewise, we have

prepared another two samples by simply varying the $\text{RuCl}_3 \cdot x\text{H}_2\text{O}$ solution to 0.015 g/L and 0.020 g/L to form Ru- Co_3O_4 15 and Ru- Co_3O_4 20 respectively.

Characterization techniques

The as-prepared samples are initially subjected to XRD analysis with a scanning rate of 5°min^{-1} in the 2θ range $10\text{-}80^\circ$ using a Bruker X-ray powder diffractometer (XRD) with Cu $K\alpha$ radiation ($\lambda = 0.154 \text{ nm}$). The morphology of the catalysts was characterized with FE-SEM instrument (SUPRA 55VP Carl Zeiss) with a separate EDS detector connected to that instrument. Energy Dispersive X-ray Spectroscopy (EDS) analysis was done with the assistance of FE-SEM instrument. X-ray photoelectron spectroscopic (XPS) analysis was performed using a Theta Probe AR-XPS system (Thermo Fisher Scientific, UK). HR-TEM, (TecnaiTM G2 TF20) working at an accelerating voltage of 200 kV and by Talos F-200-S with HAADF elemental mapping.

Electrochemical measurements

The electrochemical properties were measured using a Metrohm AUTOLAB-M240 instrument with techniques like CV, LSV, and chronoamperometry. All the electrochemical experiments were carried out by employing a conventional three-electrode set-up. (Hg/HgO and saturated calomel electrode (SCE)-reference for alkaline and acidic medium, graphite rod-counter and carbon cloth (CC)-working electrode). The working electrodes were fabricated using 1 mg of polyvinylidene fluoride (PVDF) as a binder and N-Methyl-2-pyrrolidone (NMP) as a slurry preparation agent. Typically, the $\approx 4:1$ (with respect to overall catalyst loading over the electrode surface) ratio of powder catalyst and PVDF had taken into a mortar, followed by the addition of NMP solvent with continuous mixing by a pestle. Then a certain amount of catalyst ink was fabricated over the 1 cm^2 area of the carbon cloth (CC). The amount of loaded catalyst was calculated by measuring the difference in weight of coated and uncoated carbon cloth (CC). Then,

EIS analysis of all the catalyst were done at an applied potential of 0.7 V (vs Hg/HgO) and 1.5 V (vs SCE) for pH=14 (1 M KOH), and pH=0.3 (0.5 M H₂SO₄) respectively. Likewise, chronoamperometric analysis also carried out at a potential of 0.69 V (vs Hg/HgO) and 1.5 V (vs SCE) for pH=14, pH=0.3 respectively.

For OER in 1 M KOH solution, the commercial Hg/HgO, and graphite were used as a reference and counter electrodes, respectively.

$$E_{\text{RHE}} = E_{\text{ref}} + 0.098 + 0.059\text{pH} \dots \text{equation 1}$$

For OER in 0.5 M H₂SO₄ solution, the commercial SCE and graphite were used as a reference and counter electrodes, respectively.

$$E_{\text{RHE}} = E_{\text{ref}} + 0.241 + 0.059\text{pH} \dots \text{equation 2}$$

All the potential data were converted into an RHE scale according to the following equation: all the polarization results have normalized with respect to geometrical surface area and mass. The ECSA and mass normalization of all the LSV data were done by using the following relations:

$$\text{ECSA normalization} = \text{Current density} / \text{ECSA} \dots \text{equation 3}$$

$$\text{Mass normalization} = \text{Current density} / \text{Loading} \dots \text{equation 4}$$

Overpotential

The overpotential values of all the catalysts were calculated at a benchmarking current density of 50 mA cm⁻² by employing the following relation:

$$\eta_{10}(\text{OER}) = (E_{\text{obs}} - 1.23) \text{ V versus RHE} \dots \text{equation 5}$$

$$\eta_{10}(\text{HER}) = (0 - E_{\text{obs}}) \text{ V versus RHE} \dots \text{equation 6}$$

The Tafel Slope

The Tafel slope was calculated by fitting the overpotential versus log (j) using the Tafel equation as given below:

$$\eta = b \times \log (j/j_0) \dots\dots\dots \text{equation 7}$$

where “b” signifies the Tafel slope value, “j” implies the current density value, and “j₀” is the exchange current density. Electrochemical impedance spectroscopy (EIS) measurements were done on the frequency ranges from 10⁵ to 0.1 Hz.

Electrochemical Active Surface Area (ECSA)

The electrochemical active surface areas (ECSA) were measured by determining the electrochemical C_{dl} using the following equations:

$$i_c = v \times C_{dl} \dots\dots\dots \text{equation 8}$$

$$\text{ECSA} = C_{dl}/C_s \dots\dots\dots \text{equation 9}$$

where “i_c” indicates the double-layer charging current resulting from scan-rates (v) dependent CVs at non-faradic potential, and “C_s” denotes a specific capacitance value of 0.040 mF cm⁻² depending on the typical reported values.

Turnover Frequency (TOF)

The amount of oxygen/hydrogen that is evolved per unit of time is known as the TOF. The TOF of the catalyst can be determined by the below expression,

$$\text{TOF} = \frac{j \times N_A}{n \times F \times \tau} \dots\dots\dots \text{equation 10}$$

where, j = current density, N_A = Avogadro number, F = Faraday constant (96 485 C mol⁻¹), n = Number of electrons (For OER, n = 4 and HER, n = 2), Γ = Surface concentration.

Faradaic Efficiency (FE):

For the RRDE experiment, 4 mg of Au@LaFeO₃ catalyst was added to a solution containing 750 μL of H₂O, 200 μL of ethanol, and 50 μL of 5% Nafion solution. The above mixture was probe sonicated for 20 min to prepare a homogeneous catalyst ink. Later, 15 μL of homogeneous ink was drop-casted over the GC disk of RRDE set up with an effective surface area of ≈0.197 cm². The Pt ring was used with a constant potential of 0.3V versus RHE to reduce the as-formed O₂ in situ. The FE was calculated from the ratio of the ring current to the disk using the following expression:

$$FE = I_{\text{ring}} / (I_{\text{disk}} \times N) \times 100 \dots\dots\dots\text{equation 11}$$

where, “I_{ring}” and “I_{disk}” are the ring and disk current density in mA cm⁻², respectively; “N” is the collection efficiency having a constant value of 0.249.

Determination of surface concentration, Charge over the electrode surface and TOF values of all four catalyst from the redox features of CV:^{1,2}

- Calculated area associated with the oxidation of Co²⁺ to Co³⁺ of **Co₃O₄** = 0.00003203 VA

Hence, the associated charge is = 0.00003203 VA / 0.1 Vs⁻¹

$$= 0.0003203 \text{ As}$$

$$= \mathbf{0.0003203 \text{ C}}$$

- Calculated area associated with the oxidation of Co²⁺ to Co³⁺ of **Ru-Co₃O₄ 10** = 0.0004051 VA

Hence, the associated charge is = 0.0004051 VA / 0.1 Vs⁻¹

$$= 0.004051 \text{ As}$$

$$= \mathbf{0.004051 \text{ C}}$$

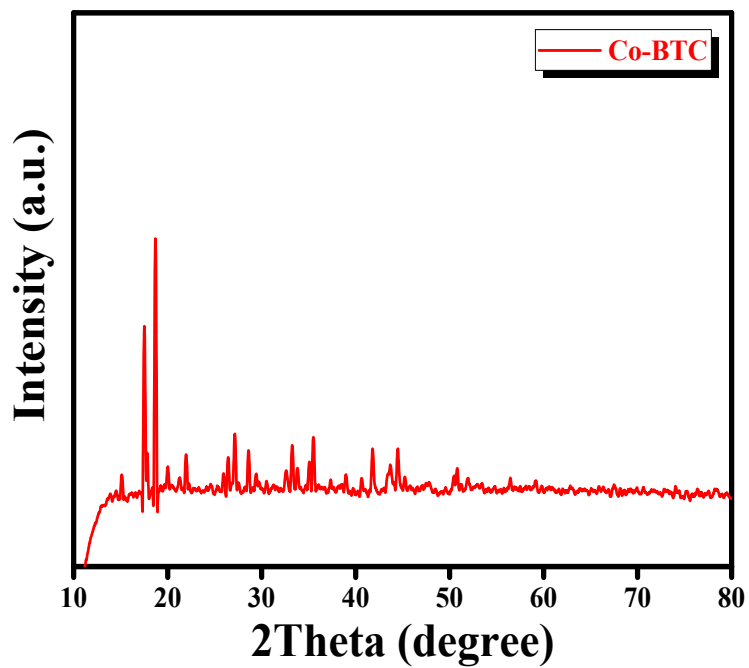


Figure S1: PXRD pattern of Co-BTC (BTC-benzene tricarboxylic acid).

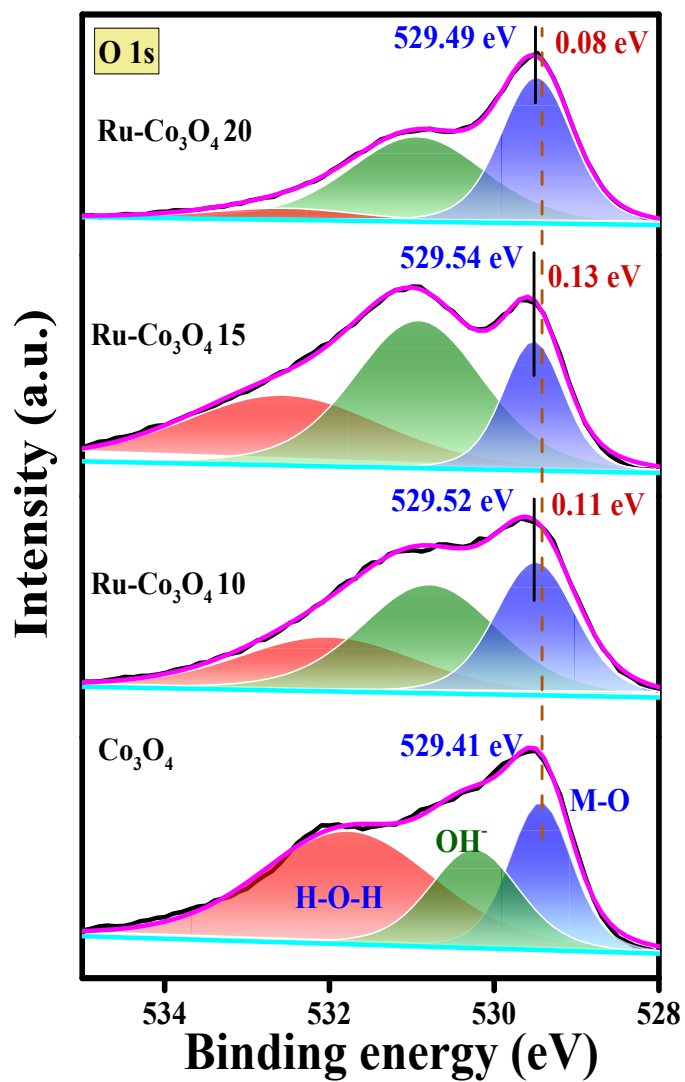


Figure S2: Deconvoluted O 1s XPS spectra of Co₃O₄, Ru-Co₃O₄ 10, Ru-Co₃O₄ 15 and Ru-Co₃O₄ 20.

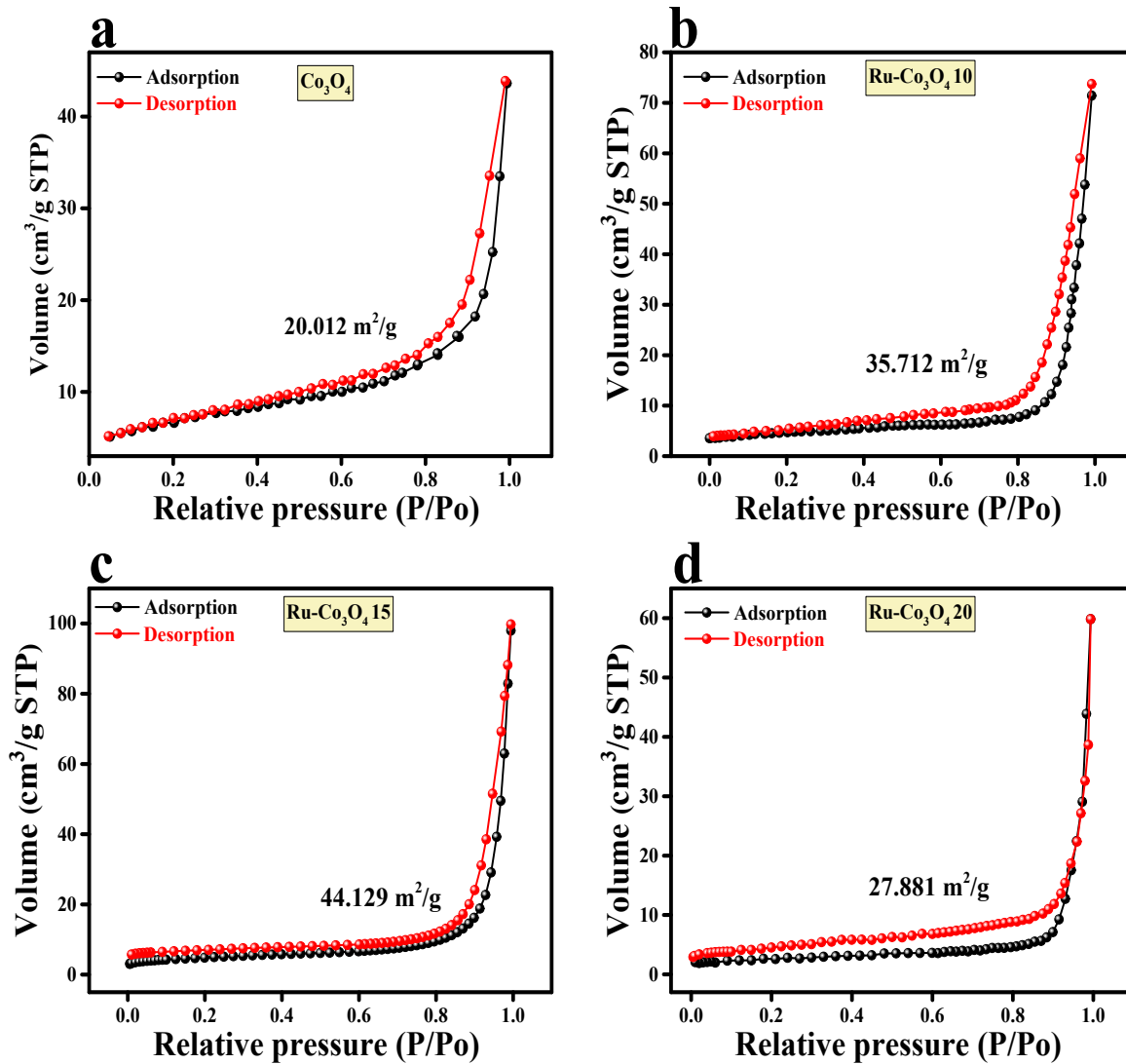


Figure S3: (a-d) N₂ adsorption-desorption of Co₃O₄, Ru-Co₃O₄ 10, Ru-Co₃O₄ 15 and Ru-Co₃O₄ 20 respectively.

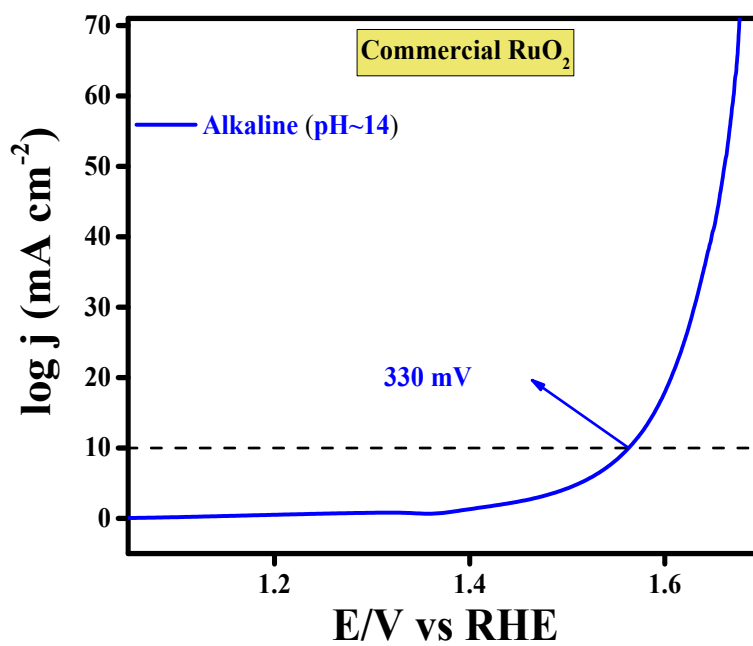


Figure S4: LSV polarization result of commercial RuO₂ in 1 M KOH electrolyte.

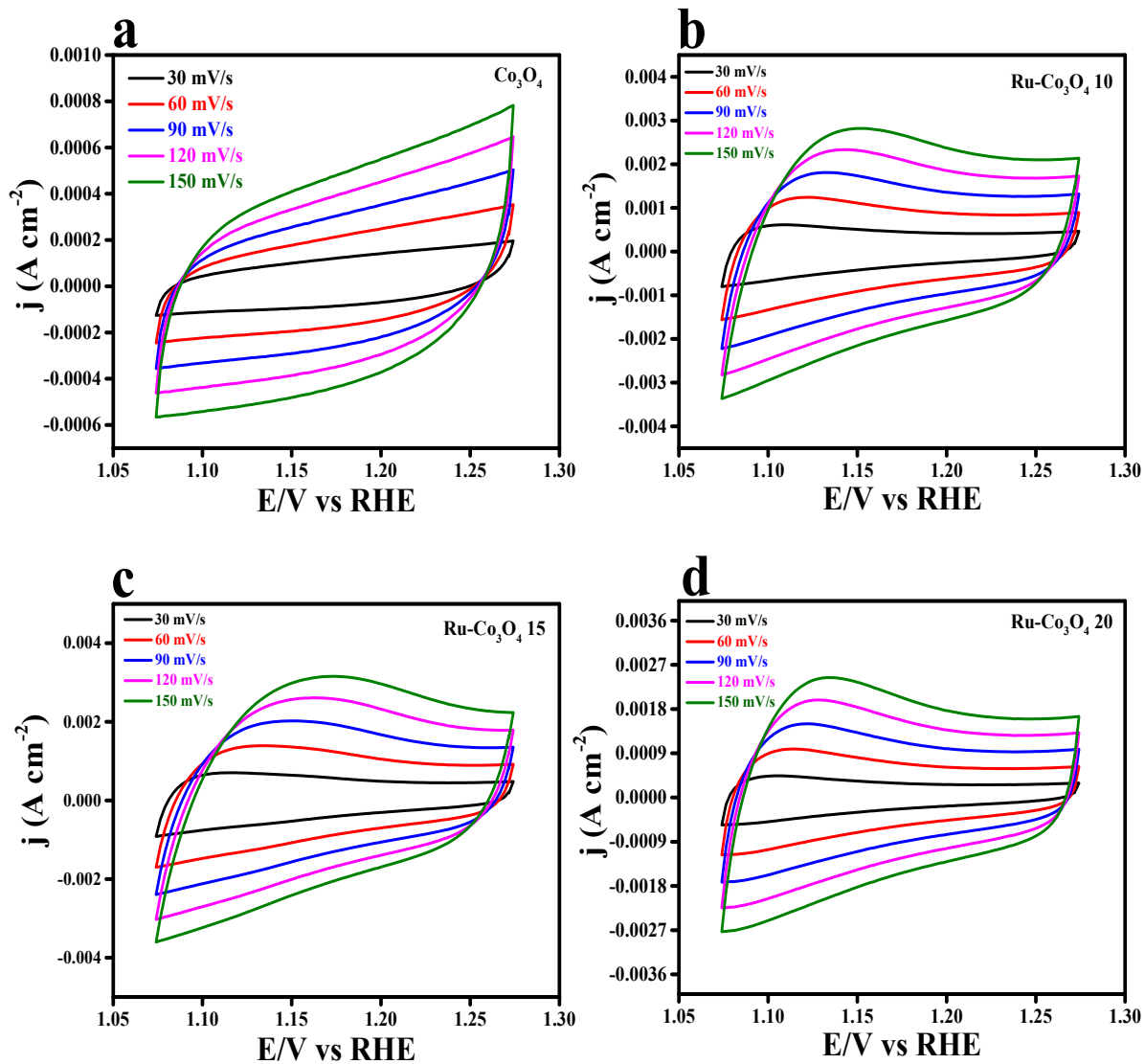


Figure S5: CVs recorded at non-faradaic region at a different scan rate for Co_3O_4 , Ru- Co_3O_4 10, Ru- Co_3O_4 15 and Ru- Co_3O_4 20 respectively in 1 M KOH electrolyte.

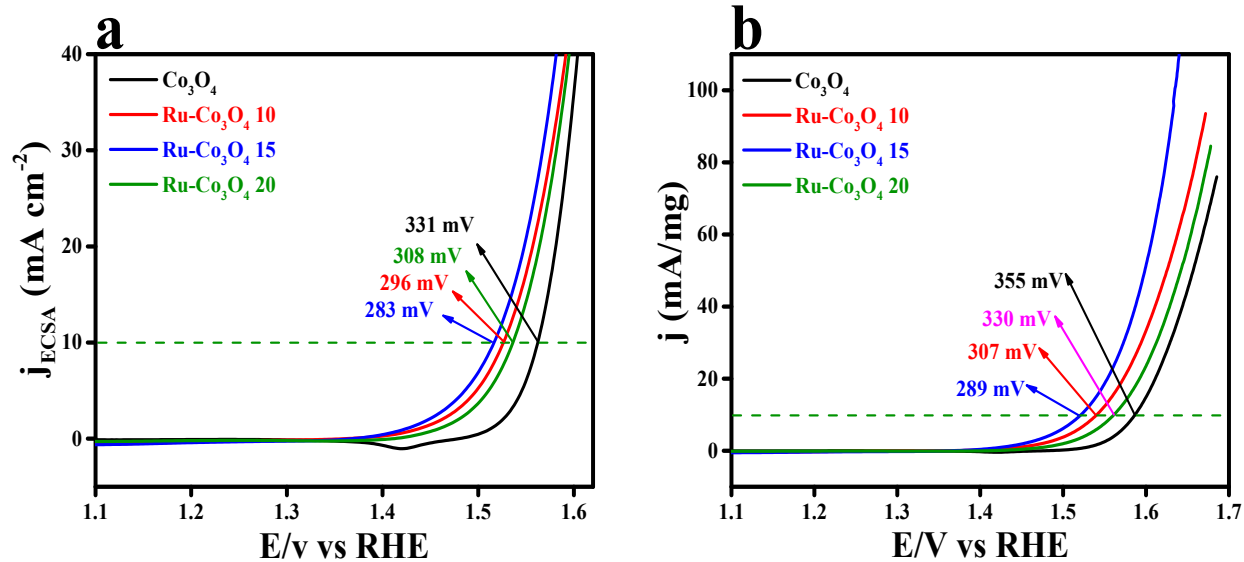


Figure S6: (a and b) ECSA normalized (specific activity) and mass dependent activity of Co_3O_4 , $\text{Ru-Co}_3\text{O}_4$ 10, $\text{Ru-Co}_3\text{O}_4$ 15 and $\text{Ru-Co}_3\text{O}_4$ 20 respectively in 1

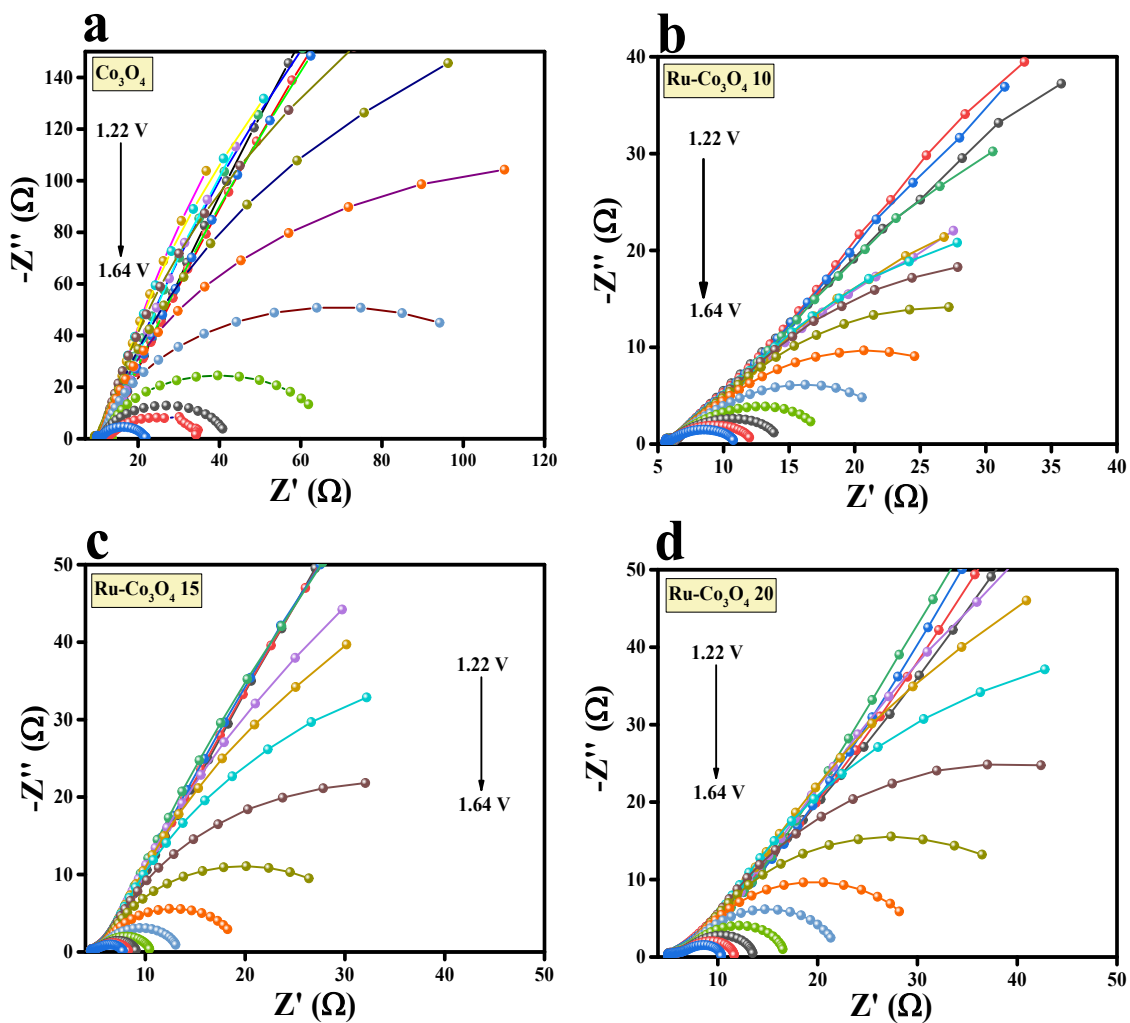


Figure S7: (a-d) Operando Nyquist plot of Co_3O_4 , $\text{Ru-Co}_3\text{O}_4$ 10, $\text{Ru-Co}_3\text{O}_4$ 15 and $\text{Ru-Co}_3\text{O}_4$ 20 respectively.

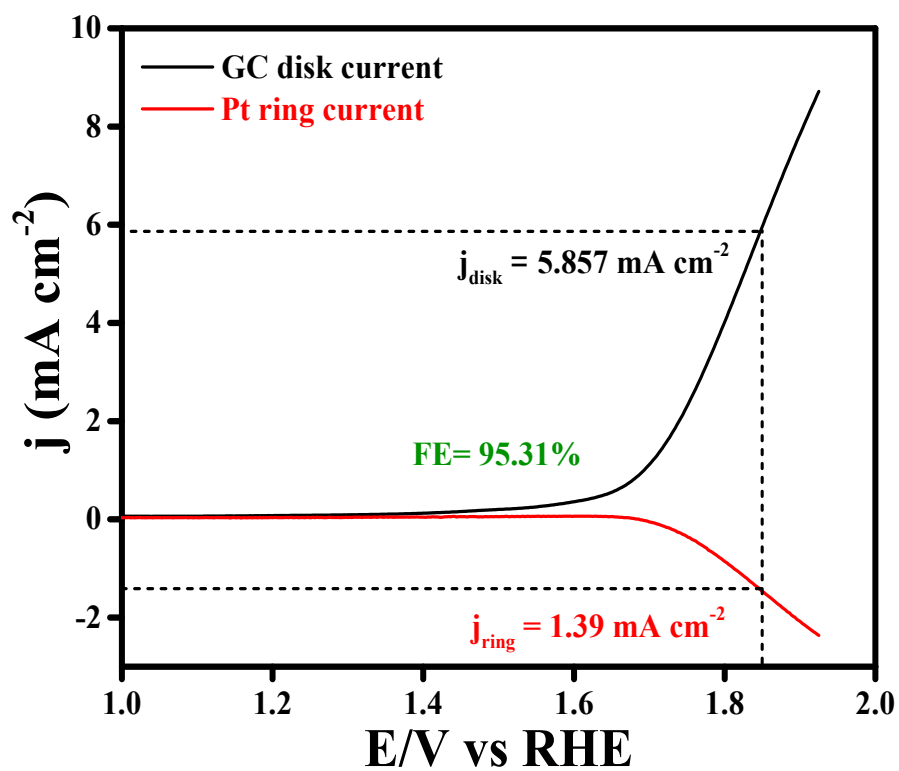


Figure S8: Faradaic efficiency (FE) of the Ru-Co₃O₄ 15 electrocatalyst for OER in 1 M KOH solution.

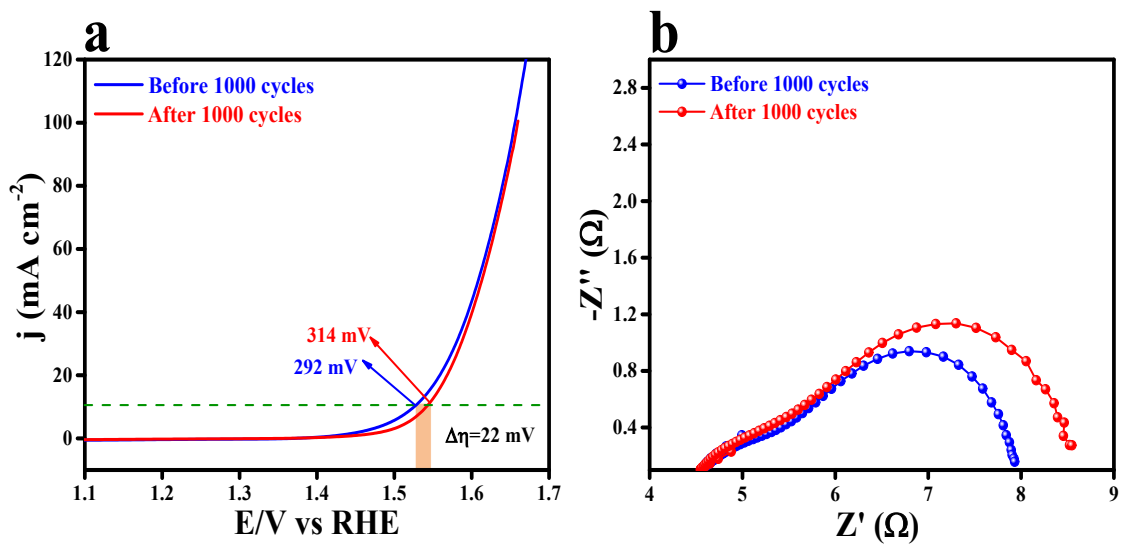


Figure S9: (a) LSV polarization curves of Ru-Co₃O₄ 15 after 1000 continuous CV cycles in 1 M KOH solution; (b) corresponding EIS analysis.

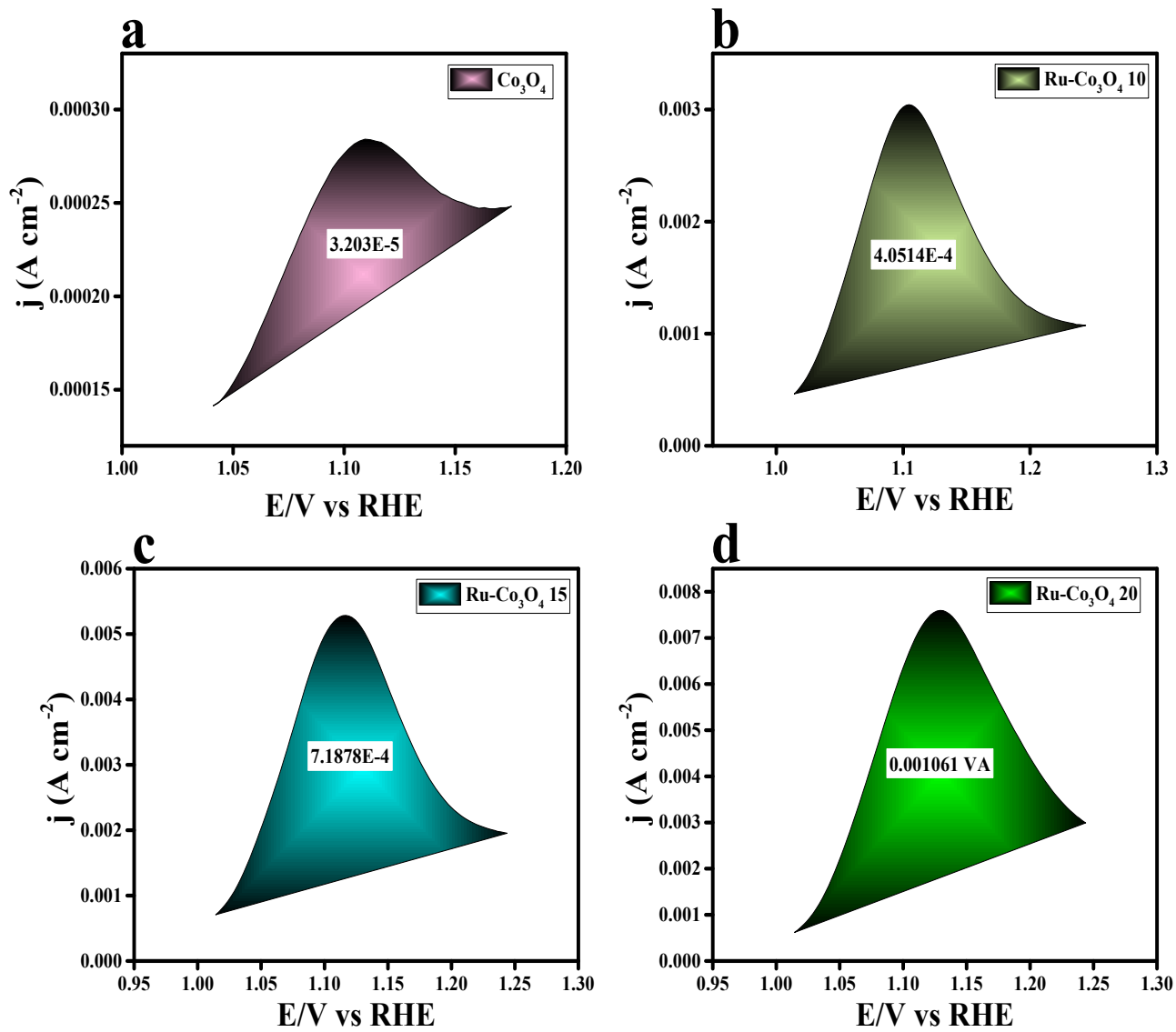


Figure S10: (a-d) Redox feature (oxidation area) of Co_3O_4 , $\text{Ru-Co}_3\text{O}_4$ 10, $\text{Ru-Co}_3\text{O}_4$ 15 and $\text{Ru-Co}_3\text{O}_4$ 20 respectively measured at 100 mV/s.

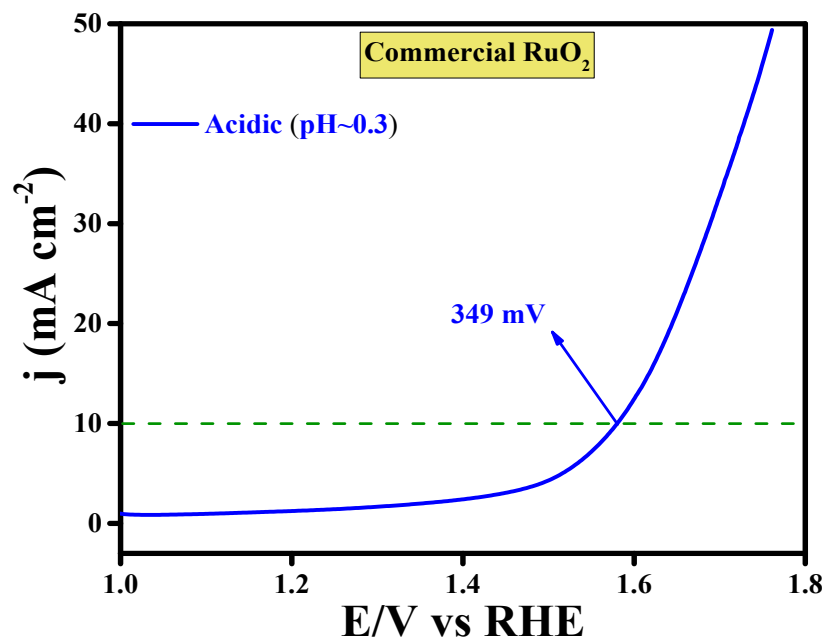


Figure S11: LSV polarization result of commercial RuO₂ in 0.5 M H₂SO₄ electrolyte.

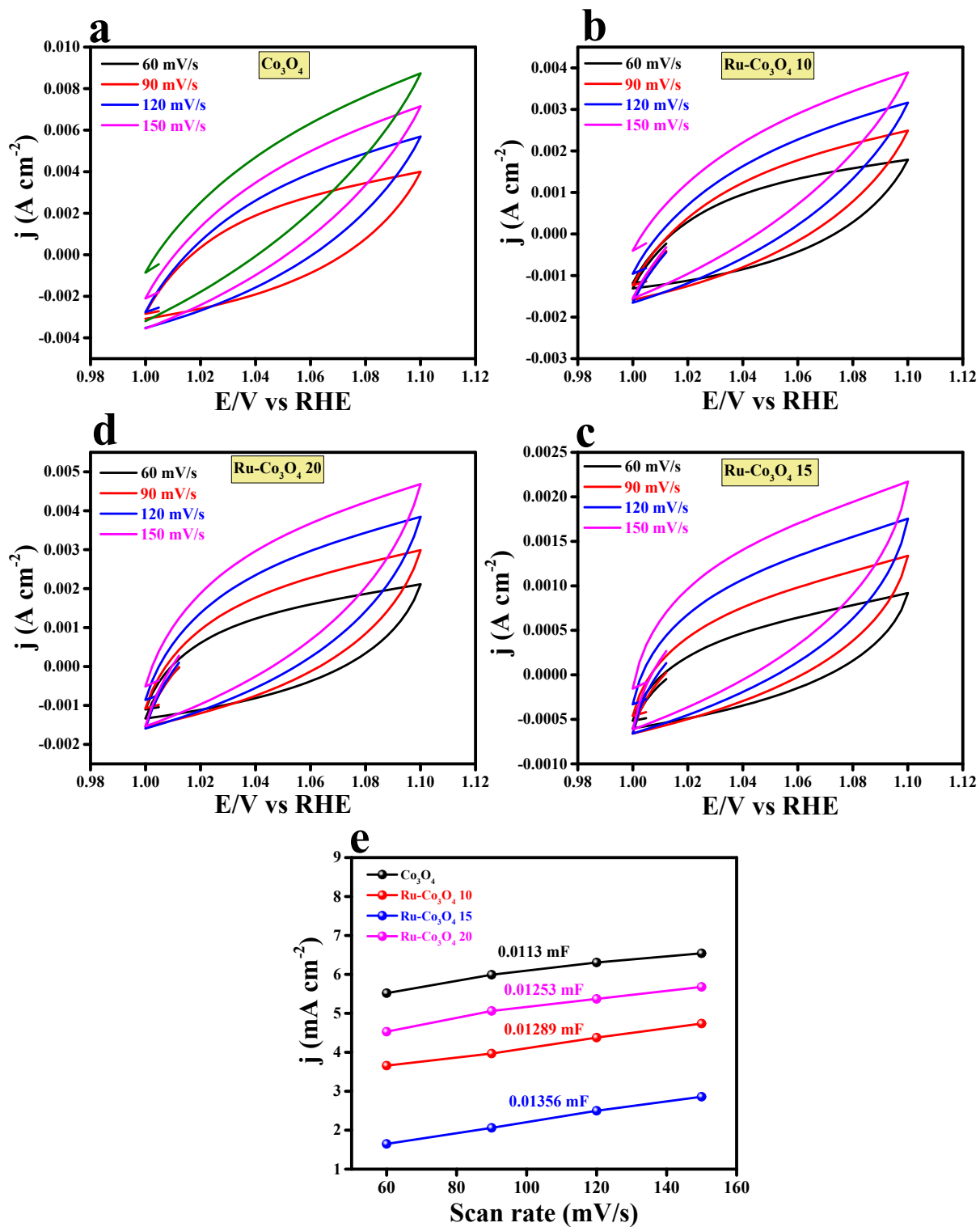


Figure S12: (a-d) CVs recorded at non-faradaic region at a different scan rate for Co₃O₄, Ru-Co₃O₄ 10, Ru-Co₃O₄ 15 and Ru-Co₃O₄ 20 respectively in 0.5 M H₂SO₄ electrolyte; (e) C_{dl}/1000 values measured from the obtained CV curves.

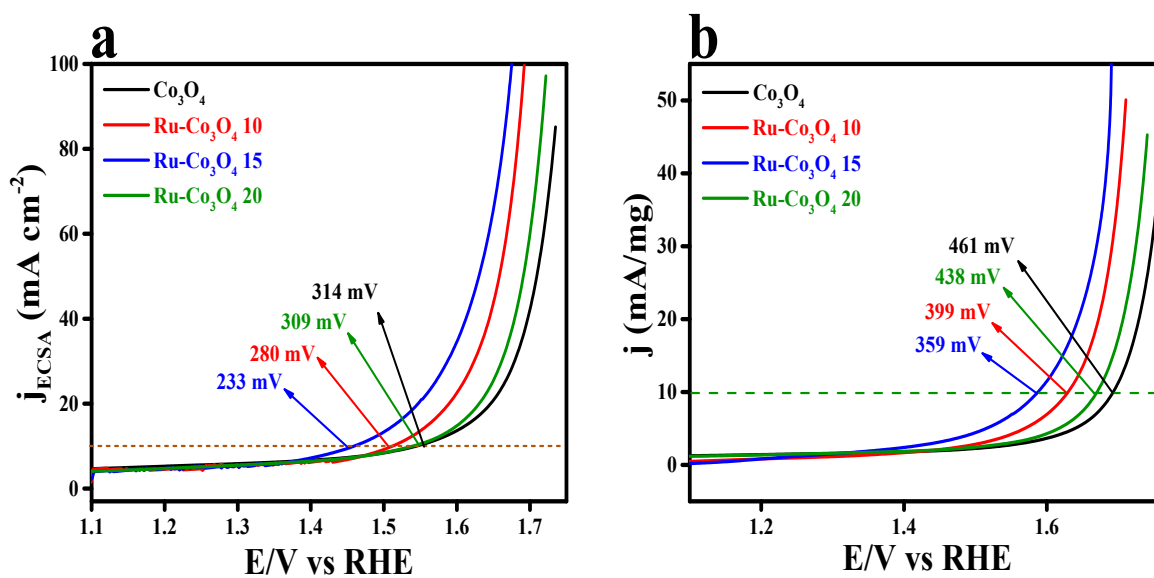


Figure S13: (a and b) ECSA normalized (specific activity) and mass dependent activity of Co_3O_4 , $\text{Ru-Co}_3\text{O}_4$ 10, $\text{Ru-Co}_3\text{O}_4$ 15 and $\text{Ru-Co}_3\text{O}_4$ 20 respectively in 0.5 M H_2SO_4 .

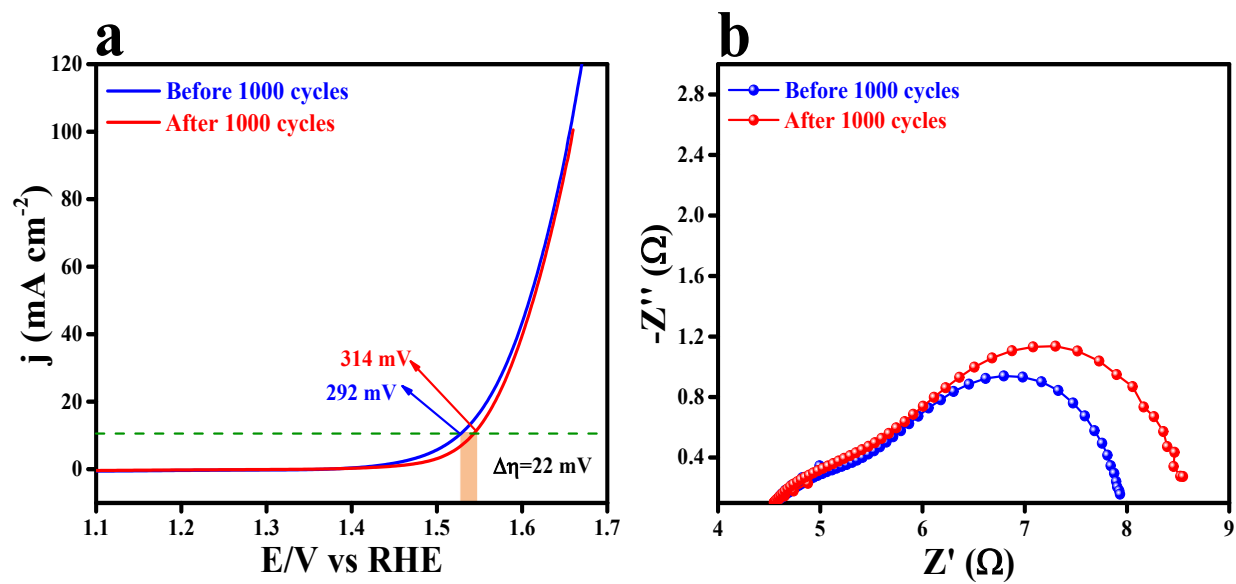


Figure S14: (a) LSV polarization curves of Ru-Co₃O₄ 15 after 1000 continuous CV cycles in 0.5 M H₂SO₄ solution; (b) corresponding EIS analysis.

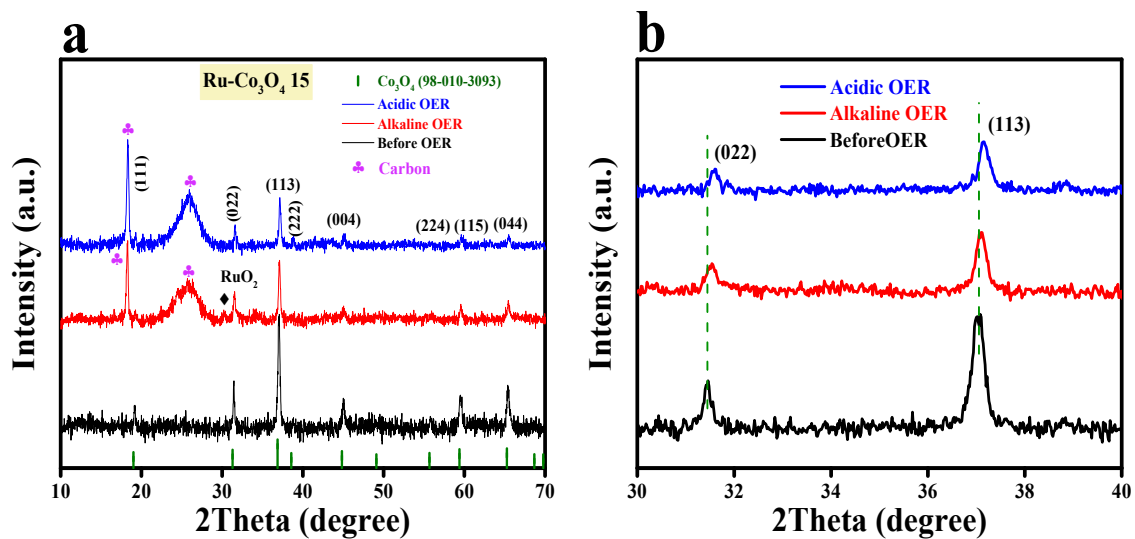


Figure S15: (a) XRD pattern of Ru-Co₃O₄ 15 before and after OER analysis in alkaline and acidic medium; (b) corresponding enlarged XRD plane of 022 and (113).

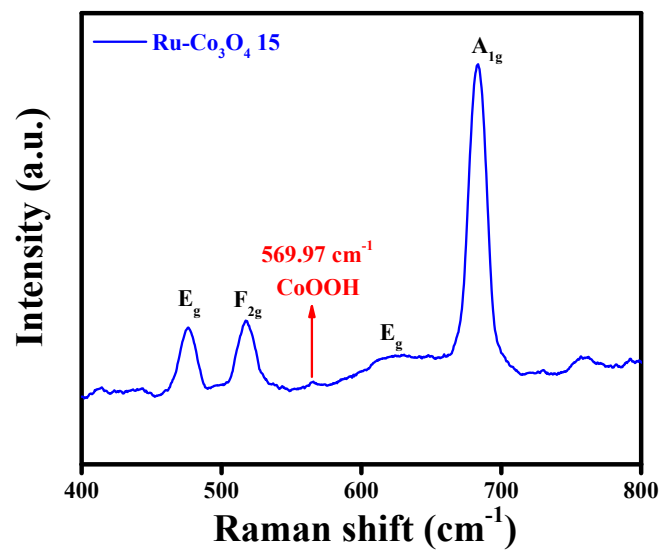


Figure S16: Post Raman spectra of Ru-Co₃O₄ in 0.5 M H₂SO₄ solution.

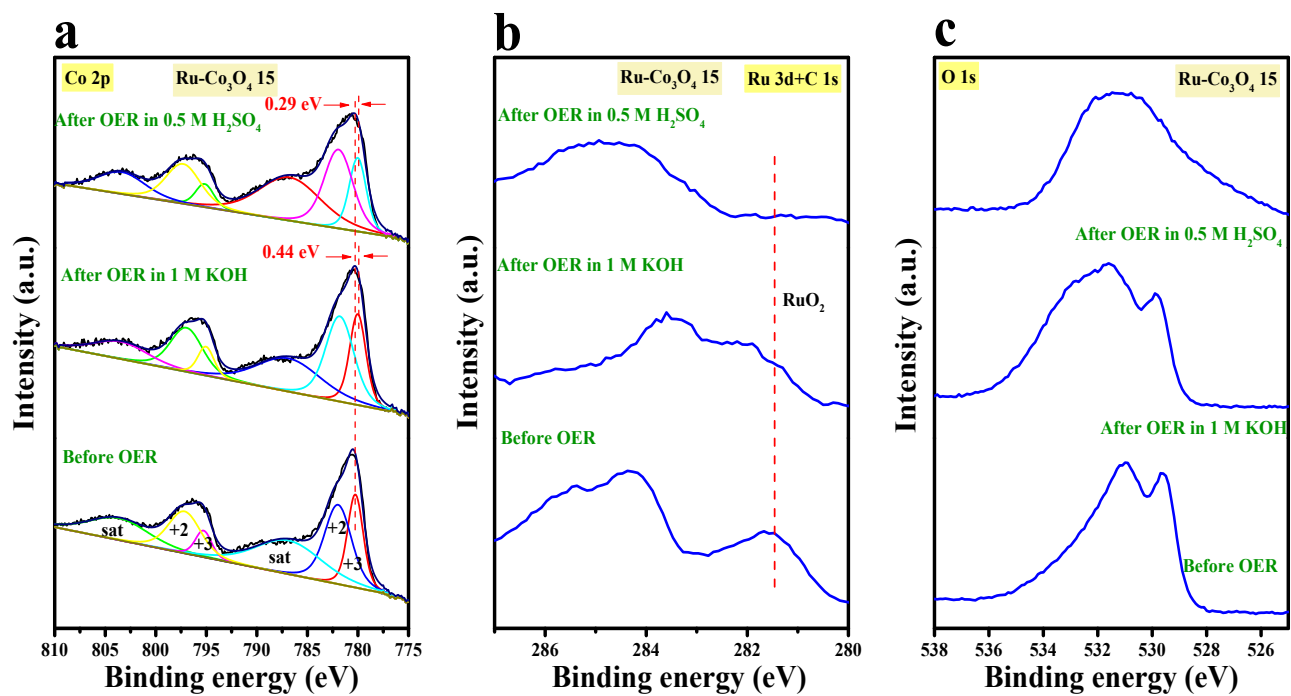


Figure S17: (a-c) Deconvoluted Co 2p XPS spectra, high resolution XPS spectra of Ru 3d+C 1s and O 1s of Ru-Co₃O₄ 15 after OER analysis in 1 M KOH and 0.5 M H₂SO₄ solution.

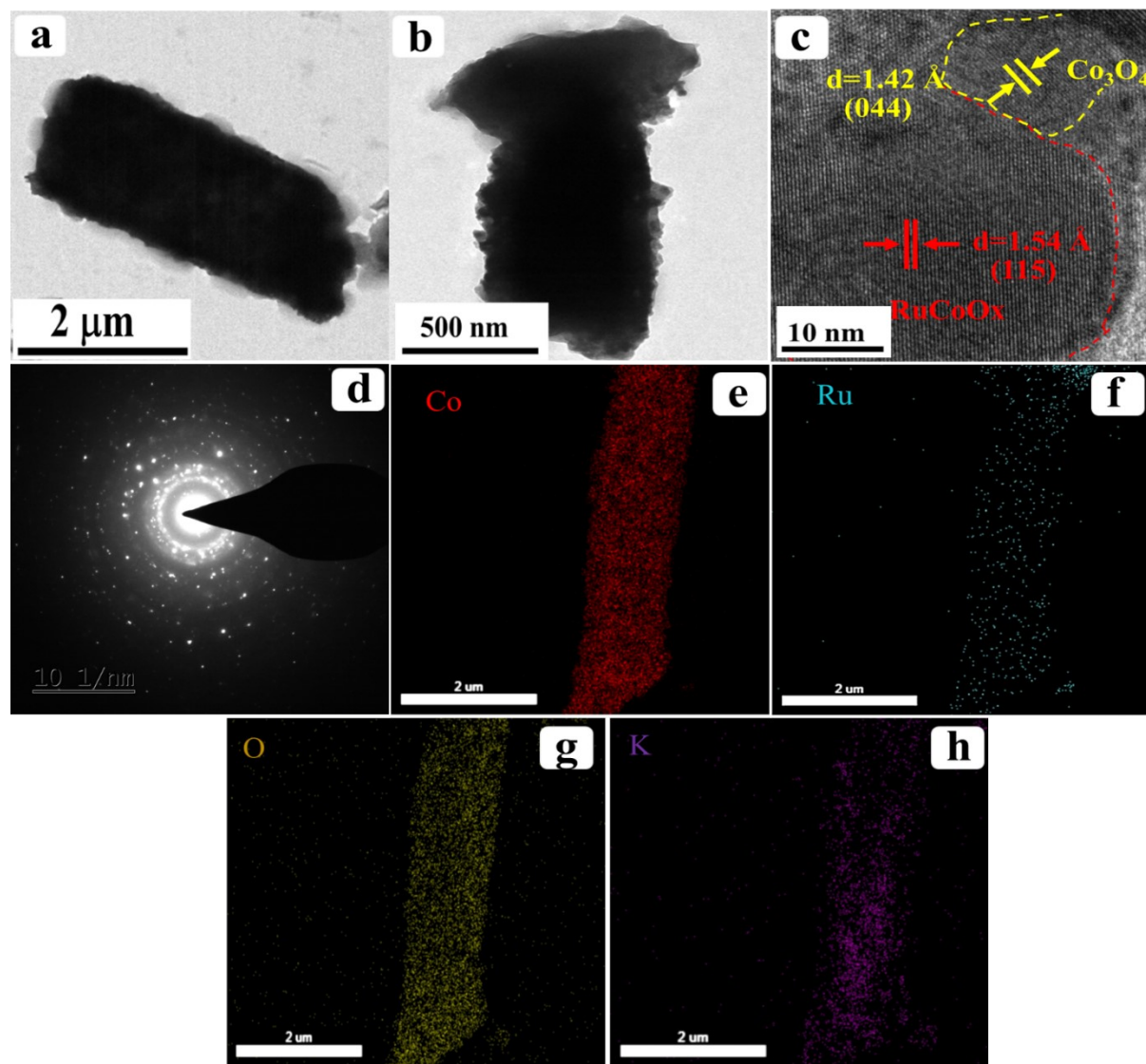


Figure S18: (a and b) Shows the low to high magnified HR-TEM images; (c and d) corresponding lattice fringes and SAED pattern; (e-h) elemental mapping results of Co, Ru, O and K of Ru-Co₃O₄ 15 after OER analysis in 1 M KOH respectively.

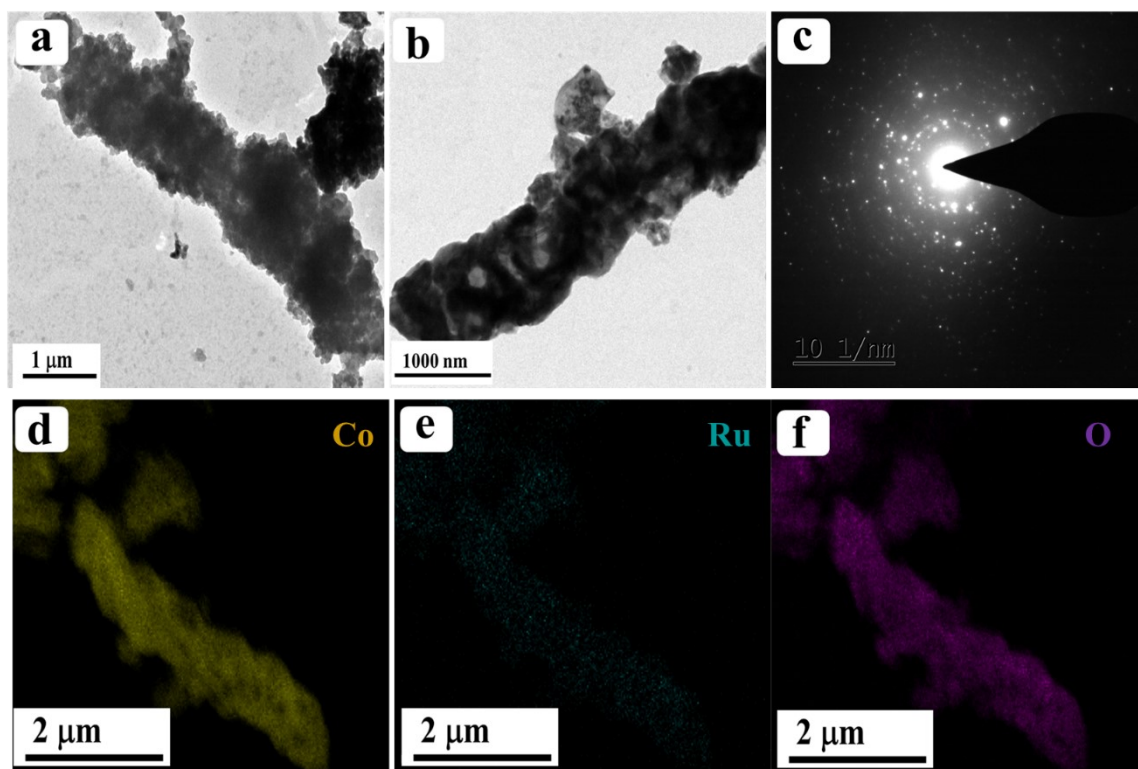


Figure S19: (a and b) Shows the low to high magnified HR-TEM images; (c) corresponding SAED pattern; (d-f) elemental mapping results of Co, Ru, O of Ru-Co₃O₄ 15 after OER analysis in 0.5 M H₂SO₄ respectively.

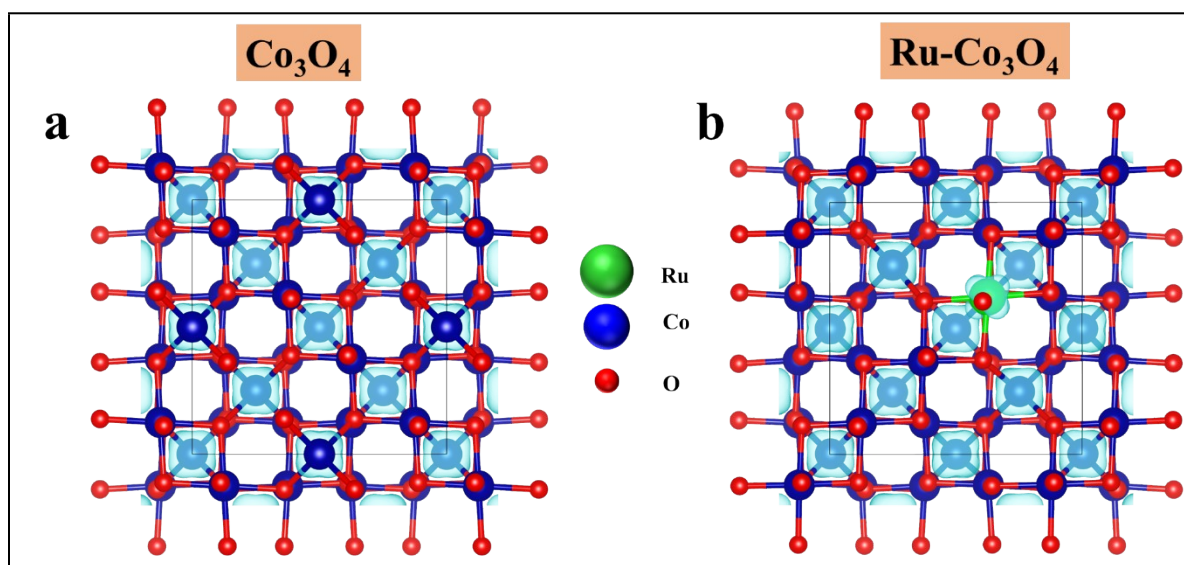


Figure S20: (a and b) Depicts the optimized electronic structure of Co_3O_4 and Ru doped Co_3O_4 respectively.

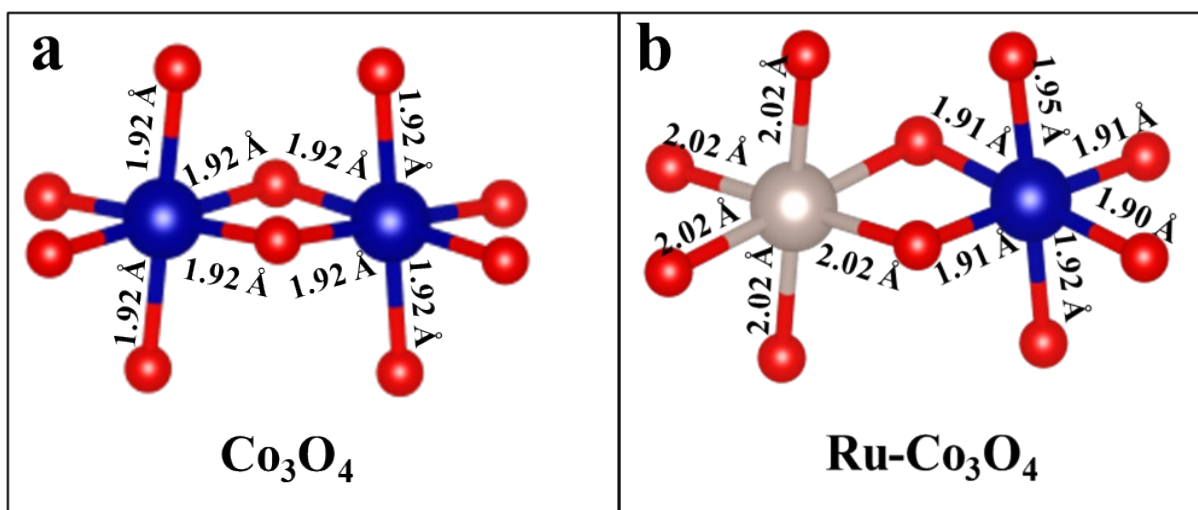


Figure S21: (a and b) Shows the determination of bond length before and after doping of Ru towards Co_3O_4 respectively.

Sl. No.	Compound	TOF@350 mV overpotential ($\times 10^{-5} \text{ s}^{-1}$)	TOF@370 mV overpotential ($\times 10^{-5} \text{ s}^{-1}$)
1	Co ₃ O ₄	1.130201	2.167435
2	Ru-Co ₃ O ₄ 10	3.236643	4.661346
3	Ru-Co ₃ O ₄ 15	4.474788	6.644037
4	Ru-Co ₃ O ₄ 20	2.059517	3.174068

Table S1: TOF values calculated at 350 and 370 mV overpotential for Co₃O₄ and various Ru-Co₃O₄ catalyst.

Sl. No.	Compound	Reduction surface area (VA)	Charge over the electrode surface (C)
1	Co ₃ O ₄	0.00003203	0.0003203
2	Ru-Co ₃ O ₄ 10	0.0004051	0.004051
3	Ru-Co ₃ O ₄ 15	0.0007187	0.007187
4	Ru-Co ₃ O ₄ 20	0.001061	0.01061

Table S2: Comparative electrochemical outcomes of Co₃O₄ and various Ru-Co₃O₄ catalyst.

Sl.No	Electrocatalyst	Substrate	Overpotential (mV)	Electrolyte (M)	Current density (mA cm ⁻²)	Reference
1	Fe-doped Co ₃ O ₄	GCE	318	1 M KOH	10 mA cm ⁻²	3
2	Mn _x Co _{3-x} O ₄	NF	218	3 M NaOH	10 mA cm ⁻²	4
3	Ru/Ni-Co ₃ O ₄	GCE	290	1 M KOH	10 mA cm ⁻²	5
4	(Ru-Co)O _x -350	GCE	265	1 M KOH	10 mA cm ⁻²	6
5	Ru@CoFe-LDH(3%)	CC	249	1 M KOH	10 mA cm ⁻²	7
6	NiCo _{1.7} Ru _{0.3} O ₄	GCE	280	1 M KOH	10 mA cm ⁻²	8
7	RuO ₂ /Co ₃ O ₄	GCE	302	1 M KOH	10 mA cm ⁻²	9
8	F _{0.2} -V-Co ₃ O ₄ -350	GCE	320	1 M KOH	10 mA cm ⁻²	10
9	Co-RuO ₂	CC	238	1 M KOH	10 mA cm ⁻²	11
10	Ru-Co₃O₄ 15	CC	292	1 M KOH	10 mA cm⁻²	This work

NF- Nickel Foam, GCE-Glassy carbon electrode, FTO-Fluorine Doped Tin Oxide Coated Glass,
CC- Carbon Cloth.

Table S3: Comparison of electrocatalytic performance of as-prepared Ru-Co₃O₄ 15 with the similar reported electrocatalyst in alkaline medium.

Sl.No	Electrocatalyst	Substrate	Overpotential (mV)	Electrolyte (M)	Current density (mA cm ⁻²)	Reference
1	Co-RuO ₂	CC	328	0.5 M H ₂ SO ₄	10 mA cm ⁻²	11
2	Co _{3-x} Ba _x O ₄	Pt wire	278	0.5 M H ₂ SO ₄	10 mA cm ⁻²	12
3	Ag-Co ₃ O ₄	FTO	370	0.5 M H ₂ SO ₄	10 mA cm ⁻²	13
4	Co ₃ O ₄ /CeO ₂	FTO	423	0.5 M H ₂ SO ₄	10 mA cm ⁻²	14
5	UfD-RuO ₂	CC	179	0.5 M H ₂ SO ₄	10 mA cm ⁻²	15
6	Y ₂ [Ru _{1.6} Y _{0.4}]O _{7-δ}	GCE	190	0.1 M HClO ₄	10 mA cm ⁻²	16
7	Ag-Co ₃ O ₄ 400	GCE	470	0.5 M H ₂ SO ₄	10 mA cm ⁻²	17
8	Li _{0.52} RuO ₂	GCE	156	0.5 M H ₂ SO ₄	10 mA cm ⁻²	18
9	Co doped RuO ₂	GCE	169	0.5 M H ₂ SO ₄	10 mA cm ⁻²	19
10	Ru-Co₃O₄ 15	CC	365	0.5 M H₂SO₄	10 mA cm⁻²	This work

GCE-Glassy carbon electrode, FTO-Fluorine Doped Tin Oxide Coated Glass, CC- Carbon Cloth.

References

- 1 S. Anantharaj and S. Kundu, *ACS Energy Lett.*, 2019, **4**, 1260–1264.
- 2 K. Karthick, S. Anantharaj, P. E. Karthik, B. Subramanian and S. Kundu, *Inorg. Chem.*, 2017, **56**, 6734–6745.
- 3 K. Min, M. Hwang, S. E. Shim, D. Lim and S. H. Baeck, *Chem. Eng. J.*, 2021, **424**, 130400.
- 4 Y. Ma, M. Zha, Y. Dong, L. Li and G. Hu, *Mater. Res. Express*, 2019, **6**, 115033.
- 5 B. Guo, R. Ma, Z. Li, J. Luo, M. Yang and J. Wang, *Mater. Chem. Front.*, 2020, **4**, 1390–1396.
- 6 C. Wang, H. Shang, J. Li, Y. Wang, H. Xu, C. Wang, J. Guo and Y. Du, *Chem. Eng. J.*, 2021, **420**, 129805.
- 7 A. Karmakar, R. Jayan, A. Das, A. Kalloorkal, M. Islam and S. Kundu, *ACS Appl. Mater. Interfaces*, 2023, **15**, 26928–26938.
- 8 C. Peng, H. Liu, J. Chen, Y. Zhang, L. Zhu, Q. Wu, W. Zou, J. Wang, Z. Fu and Y. Lu, *Appl. Surf. Sci.*, 2021, **544**, 148897.
- 9 B. Y. Guo, X. Y. Zhang, X. Ma, T. S. Chen, Y. Chen, M. L. Wen, J. F. Qin, J. Nan, Y. M. Chai and B. Dong, *Int. J. Hydrogen Energy*, 2020, **45**, 9575–9582.
- 10 J. Y. Xie, R. Y. Fan, J. Y. Fu, Y. N. Zhen, M. X. Li, H. J. Liu, Y. Ma, F. L. Wang, Y. M. Chai and B. Dong, *Int. J. Hydrogen Energy*, 2021, **6**, 1–9.
- 11 R. Madhu, A. Karmakar, S. Kumaravel, S. S. Sankar, K. Bera, S. Nagappan, H. N. Dhandapani and S. Kundu, *ACS Appl. Mater. Interfaces*, 2022, **14**, 1077–1091.
- 12 N. Wang, P. Ou, R. K. Miao, Y. Chang, Z. Wang, S. F. Hung, J. Abed, A. Ozden, H. Y. Chen, H. L. Wu, J. E. Huang, D. Zhou, W. Ni, L. Fan, Y. Yan, T. Peng, D. Sinton, Y. Liu, H. Liang and E. H. Sargent, *J. Am. Chem. Soc.*, 2023, **14**, 7829–7836.
- 13 K. L. Yan, J. Q. Chi, J. Y. Xie, B. Dong, Z. Z. Liu, W. K. Gao, J. H. Lin, Y. M. Chai and C.

- G. Liu, *Renew. Energy*, 2018, **119**, 54–61.
- 14 J. Huang, H. Sheng, R. D. Ross, J. Han, X. Wang, B. Song and S. Jin, *Nat. Commun.*, 2021, **12**, 3036.
- 15 R. Ge, L. Li, J. Su, Y. Lin, Z. Tian and L. Chen, *Adv. Energy Mater.*, 2019, **9**, 1–9.
- 16 J. Kim, P. C. Shih, Y. Qin, Z. Al-Bardan, C. J. Sun and H. Yang, *Angew. Chemie - Int. Ed.*, 2018, **57**, 13877–13881.
- 17 K. L. Yan, J. F. Qin, J. H. Lin, B. Dong, J. Q. Chi, Z. Z. Liu, F. N. Dai, Y. M. Chai and C. G. Liu, *J. Mater. Chem. A*, 2018, **6**, 5678–5686.
- 18 Y. Qin, T. Yu, S. Deng, X. Y. Zhou, D. Lin, Q. Zhang, Z. Jin, D. Zhang, Y. B. He, H. J. Qiu, L. He, F. Kang, K. Li and T. Y. Zhang, *Nat. Commun.*, 2022, **13**, 3784.
- 19 Y. Tian, S. Wang, E. Velasco, Y. Yang, L. Cao, L. Zhang, X. Li, Y. Lin, Q. Zhang and L. Chen, *iScience*, 2020, **23**, 100756.